Electronic Supplementary Material (ESI) for Dalton Transactions.

Supplementary Information

A chiral spirobifluorene-based bis(salen) zinc(II) receptor towards highly enantioselective binding of chiral carboxylates

Sk Asif Ikbal,[a] Yoko Sakata[a,b] and Shigehisa Akine[a,b]

[a] Nano Life Science Institute (WPI-NanoLSI), Kanazawa University

[b] Graduate School of Natural Science and Technology, Kanazawa University

Experimental Section

Materials. (*R*)-(–)-2,3-diaminopropionic acid hydrochloride was commercially purchased from TCI and amine groups were protected by *tert*-butyloxycarbonyl (Boc) groups by reported procedure.[1] We have synthesized 2,2′-diamino-9,9′-spirobifluorene, (*rac*)-**1**, according to the literature procedures.[2] Other reagents and solvents were purchased from commercial sources and purified by standard procedures before use.

Synthesis of (*R*,*rac*,*R*)-2.

A mixture of 2,2′-diamino-9,9′-spirobifluorene, ((*rac*)-**1**) (100.0 mg, 0.288 mmol) and Boc-protected (*R*)-(–)-2,3-diaminopropanoic acid (351.3 mg, 1.153 mmol) were dissolved in dry DMF (6 mL) under nitrogen atmosphere. Dry hydroxybenzotriazole (HOBT) (156.0 mg, 1.153 mmol) and 1-ethyl-3-(3-dimethylaminopropyl)carbodiimide (EDC) (221.3 mg, 1.153 mmol) were added to the reaction mixture, which was stirred at room temperature for 2 days. The solution was concentrated to dryness and diluted with ethyl acetate. The solution was washed with 2% aqueous HCl solution followed by sodium bicarbonate solution and the organic layer was dried over anhydrous sodium sulfate. The solution was concentrated to dryness to yield solid powder. The crude product was subjected to column chromatography on silica gel (100–200 mesh) with ethyl acetate/hexane (50:50). The first fraction (RF = 0.36) was in negligible amount (~ 1.0 mg) and was free diamine. The second fraction (RF = 0.26) was characterized as the mono-amide bifluorene product (light yellow solid, 25.8 mg). The third fraction (RF = 0.13) is impure mixture product (45.7 mg), whereas the last fraction (RF = 0.10) was characterized as the targeted bis-amide bifluorene product (light yellow solid, 67.8 mg, 25.6%). ^{1}H NMR ($CDCl_3$, 298 K) δ 8.72 (br, 2H, NH), 7.78 (d, 4H, ArH), 7.64 (br, 2H, ArH), 7.36 (m, 2H, ArH), 7.09 (t, 2H, ArH), 6.80 (m, 2H, ArH), 6.71 (d, 2H, ArH), 5.80 (br, 2H, NH), 5.15 (br, 2H, NH), 4.24 (m, 2H, CH), 3.47 (m, 4H, CH_2), 1.40 (s, 18H, CH_3), 1.37 (s, 18H, CH_3). The coupling constants were not relilably determined due to the presence of (*R*,*R*,*R*) and (*R*,*S*,*R*) diastereomers.

Synthesis of (*R*,*rac*,*R*)-3.

In a round bottomed flask, compound (*R,rac,R*)-**2** (150 mg, 0.162 mmol) was taken and dissolved in dry dichloromethane under nitrogen atmosphere. To the reaction mixture, trifluoroacetic acid (1 mL) was added and the resulting solution was stirred at room temperature

for overnight. The reaction mixture was diluted with ethyl acetate (20 mL) and washed with 10% aqueous NaOH solution and brine successively. The organic layer was concentrated to dryness to give white powder product, which was further recrystalized from ethyl acetate/hexane. The compound is directly used for the next step without further purification. Yield: 34.7 mg (white powder, 0.065 mmol, 41%). ^{1}H NMR ($CDCl_3$, 298 K) δ 9.69 (s, 2H, NH), 7.95 (m, 2H, ArH), 7.83 (m, 4H, ArH), 7.37 (t, 2H, ArH), 7.10 (t, 2H, ArH), 6.72 (m, 4H, ArH), 3.36 (m, 2H, CH), 3.11 (dd, 2H, CH_2), 2.93 (dd, 2H, CH_2).

Synthesis of (*R*,*rac*,*R*)-H_4L.

In a vial, (*R,rac,R*)-**3** (34.7 mg, 0.066 mmol) and 2-hydroxy-5-methylbenzaldehyde (45.49 mg, 0.334 mmol, 5 equiv) were taken and dissolved in dry DMSO (2 mL). The reaction mixture was heated at 50 °C for overnight. Chloroform (10 mL) was added to the solution, which was washed with water (5 mL × 3). The organic layer was collected, dried over anhydrous sodium sulfate, and the solvent was removed under reduced pressure. The solid compound was recrystalized with chloroform/hexane to get yellowish pure product. Yield: 26.1 mg (0.0262 mmol, 39.2%). ^{1}H NMR (DMSO-d_6, 298 K) δ 12.72 (br, 2H, OH), 12.50 (br, 2H, OH), 10.05 (br, 2H, NH), 8.48 (m, 4H, CH), 7.96 (d, 4H, ArH), 7.80 (m, 2H, ArH), 7.39 (m, 2H, ArH), 7.20 (d, 2H, ArH), 7.16 (d, 2H, ArH), 7.13–7.06 (m, 6H, ArH), 6.86 (m, 2H, ArH), 6.76–6.66 (m, 4H, ArH), 6.62 (d, 2H, ArH), 4.31 (m, 2H, CH), 4.08 (m, 2H, CH_2), 3.90 (m, 2H, CH_2), 2.19 (s, 12H, CH_3). ESI-MS: *m*/*z* 991.4211 ([(*R,rac,R*)-H_4L + H]$^+$). Anal. Calcd for $C_{63}H_{54}N_6O_6$•0.4$CHCl_3$•0.7hexane: C, 73.86; H, 5.89; N, 7.65. Found: C, 73.99; H, 5.72; N, 7.71.

Preparation of (*R*,*rac*,*R*)-LZn_2

(*R*-*rac*-*R*)-H_4L (4.6 mg, 0.0046 mmol) was dissolved in DMSO-d_6 (0.5 mL). For deprotonation of the phenolic-OH, DABCO (2.0 mg, 0.184 mmol, 4 equiv) was added to this solution. Zinc(II) trifluoromethanesulfonate (3.4 mg, 0.0092 mmol, 2 equiv) was added to the reaction mixture and stirred for 1 hour at room temperature. The solution changed to yellowish brown color and directly submitted for ^{1}H NMR analysis. ^{1}H NMR (DMSO-d_6, 298 K) δ 9.85 (s, 1H, NH), 9.83 (s, 1H, NH), 8.30–8.29 (m, 4H, CH), 7.93–7.92 (d, 4H, ArH), 7.68 (dt, 2H, ArH), 7.38–7.35 (dt, 2H, ArH), 7.09 (dt, 2H, ArH), 6.98–6.90 (m, 6H, ArH), 6.87 (d, 4H,

ArH), 6.60 (d, 2H, ArH), 6.51 (d, 4H, ArH), 4.34 (m, 2H, CH), 3.85 (m, 4H, CH_2), 2.12 (br, 12H, CH_3). ESI-MS: *m*/*z* 1119.2465 ([(*R,rac,R*)-LZn_2 + H]$^+$).

General procedure for the spectroscopic titration of (*R,rac,R*)-LZn_2 with carboxylate guests.

(*R*-*rac*-*R*)-H_4L (8.0 mg) was dissolved in $CHCl_3$/CH_3CN (1:1, 5 mL) to prepare a 1.6 mM solution. Similarly, DABCO (28.5 mg) was dissolved in $CHCl_3$/CH_3CN (1:1, 5 mL) to prepare a 46 mM solution and ZnOTf (10.4 mg) was dissolved in $CHCl_3$/CH_3CN (1:1, 5 mL) to prepare a 5.72 mM solution. Then, the solutions of (*R,rac,R*)-H_4L (2250 μL), DABCO (313 μL), and ZnOTf (1258 μL) were mixed to prepare 0.942 mM (*R,rac,R*)-LZn_2 stock solution (3.82 mL). A stock solution of guest in $CHCl_3$/CH_3CN (1:1, 28 mM, 5 mL) was separately prepared. The solution of the LZn_2 (0.942 mM, 0.127 mL), DABCO (46 mM, 0–71.7 μL; 0–5 equiv), and guest (28 mM 0-120 equiv) were mixed and then the volume of each solution was adjusted to 3.0 mL by the addition of appropriate amount of $CHCl_3$/CH_3CN (1:1) to give 0.04 mmol host concentration. The UV-vis absorption spectra and CD spectra were recorded using a quartz cell with a 10-mm path length at 298 K.

References:

1. H. Sun, H. Li, J. Wang and G. Song, *Chin. Chem. Lett.*, 2018, **29**, 977–980.
2. R. Tamura, T. Kawata, Y. Hattori, N. Kobayashi and M. Kimura, *Macromolecules*, 2017, **50**, 7978–7983.

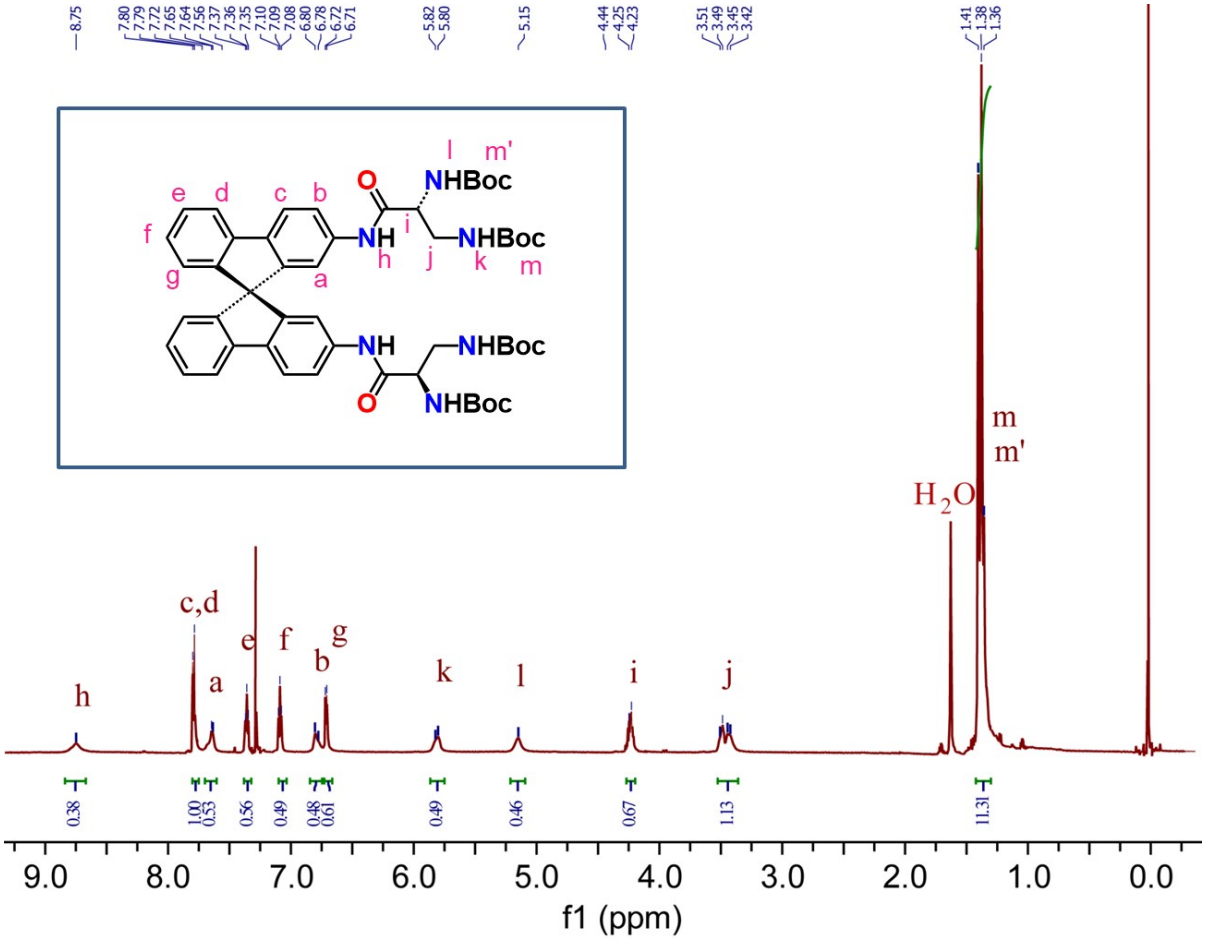

Figure S1. ^{1}H NMR spectrum of (*R,rac,R*)-**2** (600 MHz, $CDCl_3$, 298 K). Inset shows the signal assignments.

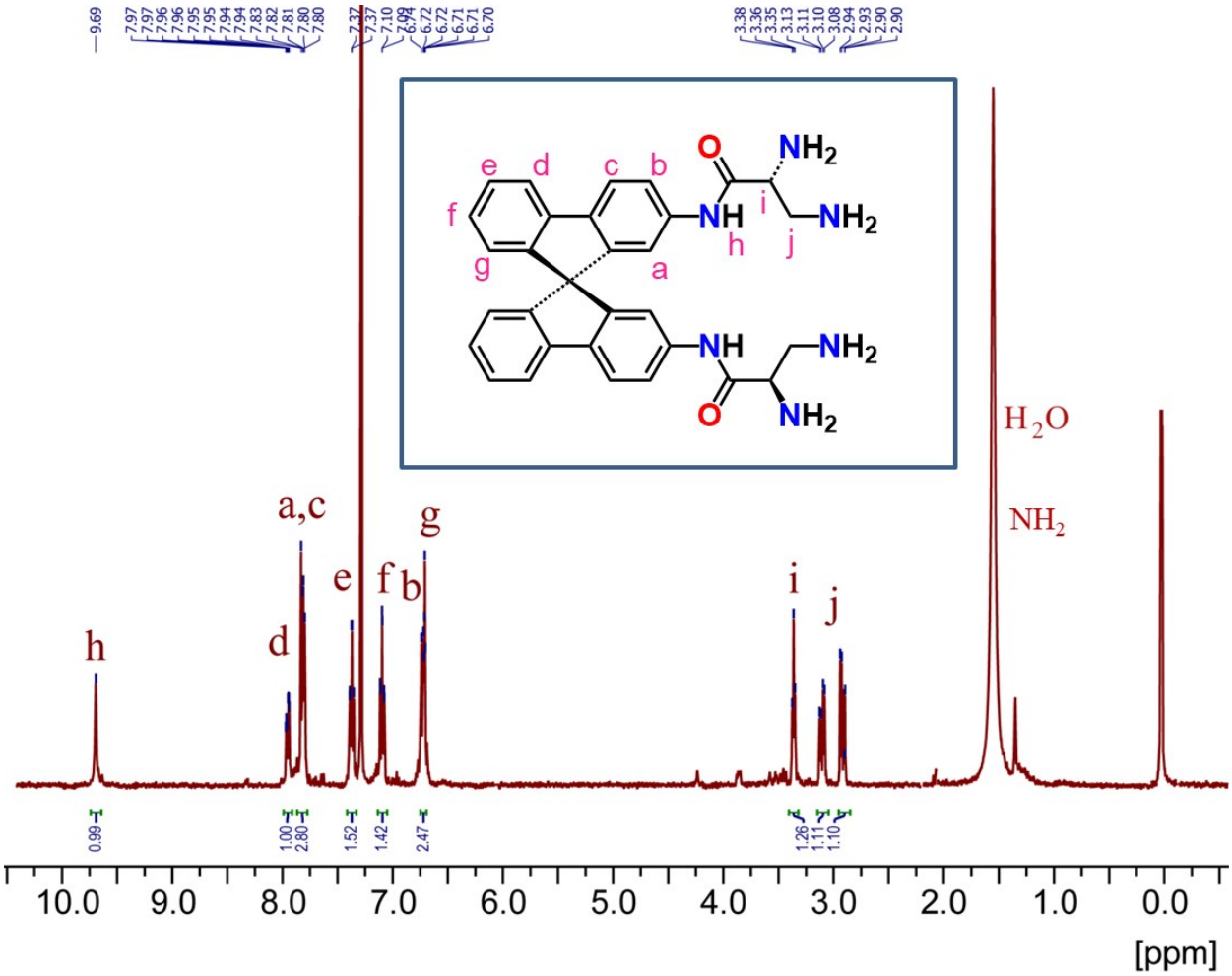

Figure S2. ^{1}H NMR spectrum of (*R,rac,R*)-**3** (600 MHz, $CDCl_3$, 298 K). Inset shows the signal assignments.

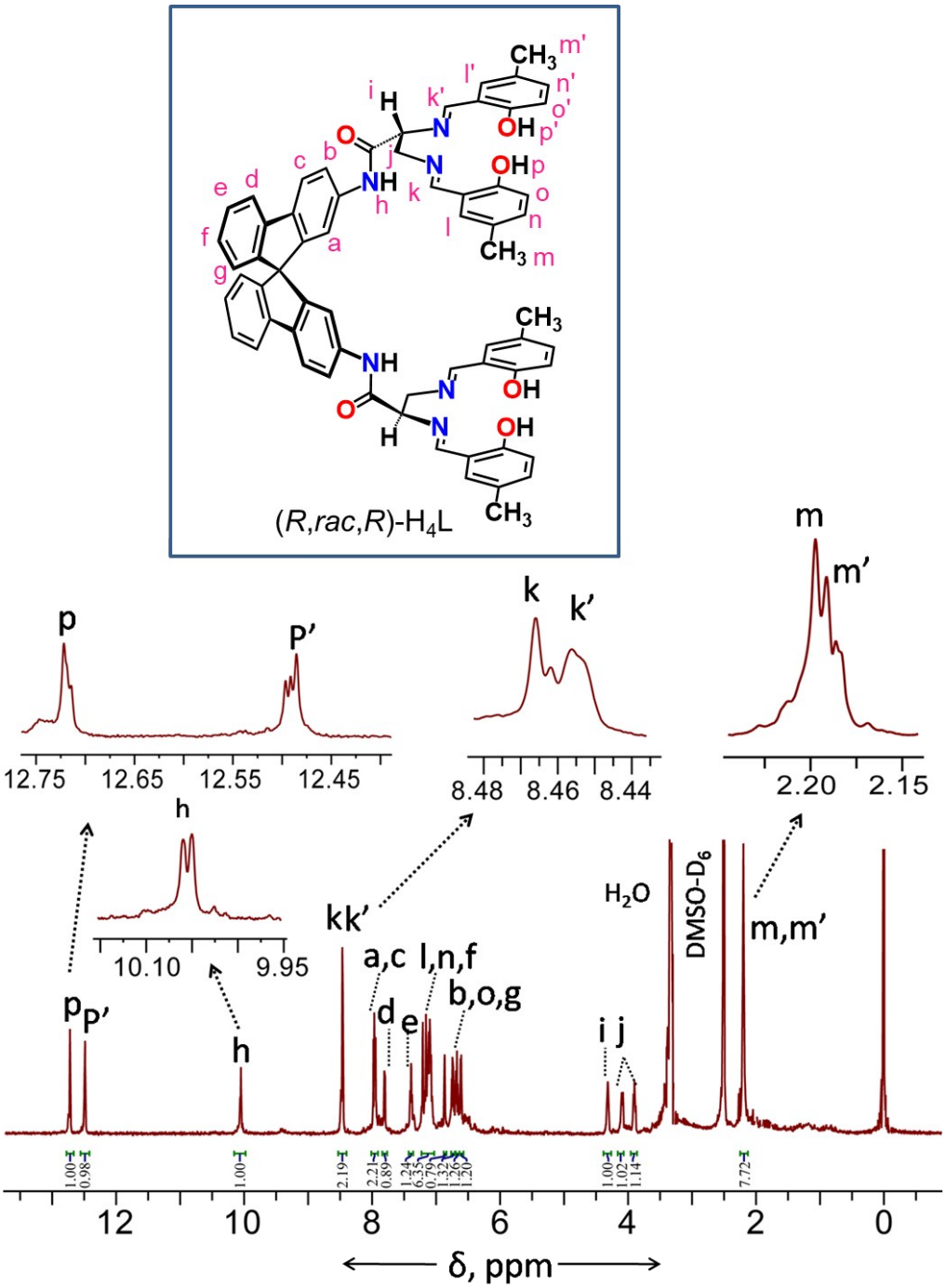

Figure S3. ^{1}H NMR spectrum of (*R,rac,R*)-H_4L (600 MHz, DMSO-d_6, 295 K). Inset shows two isomers (*R,R,R*)-H_4L and (*R,S,R*)-H_4L and the signal assignments. Signals of diastereomers can be seen as indicated in the insets.

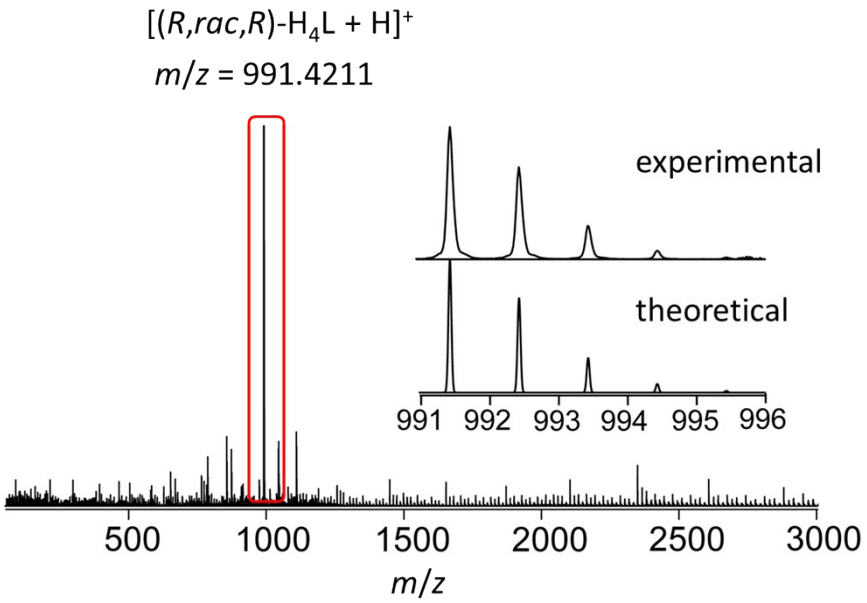

Figure S4. ESI-TOF mass spectrum of [(*R,rac,R*)-H_4L] in CH_3CN in positive mode. Inset shows the experimental and theoretical isotope patterns.

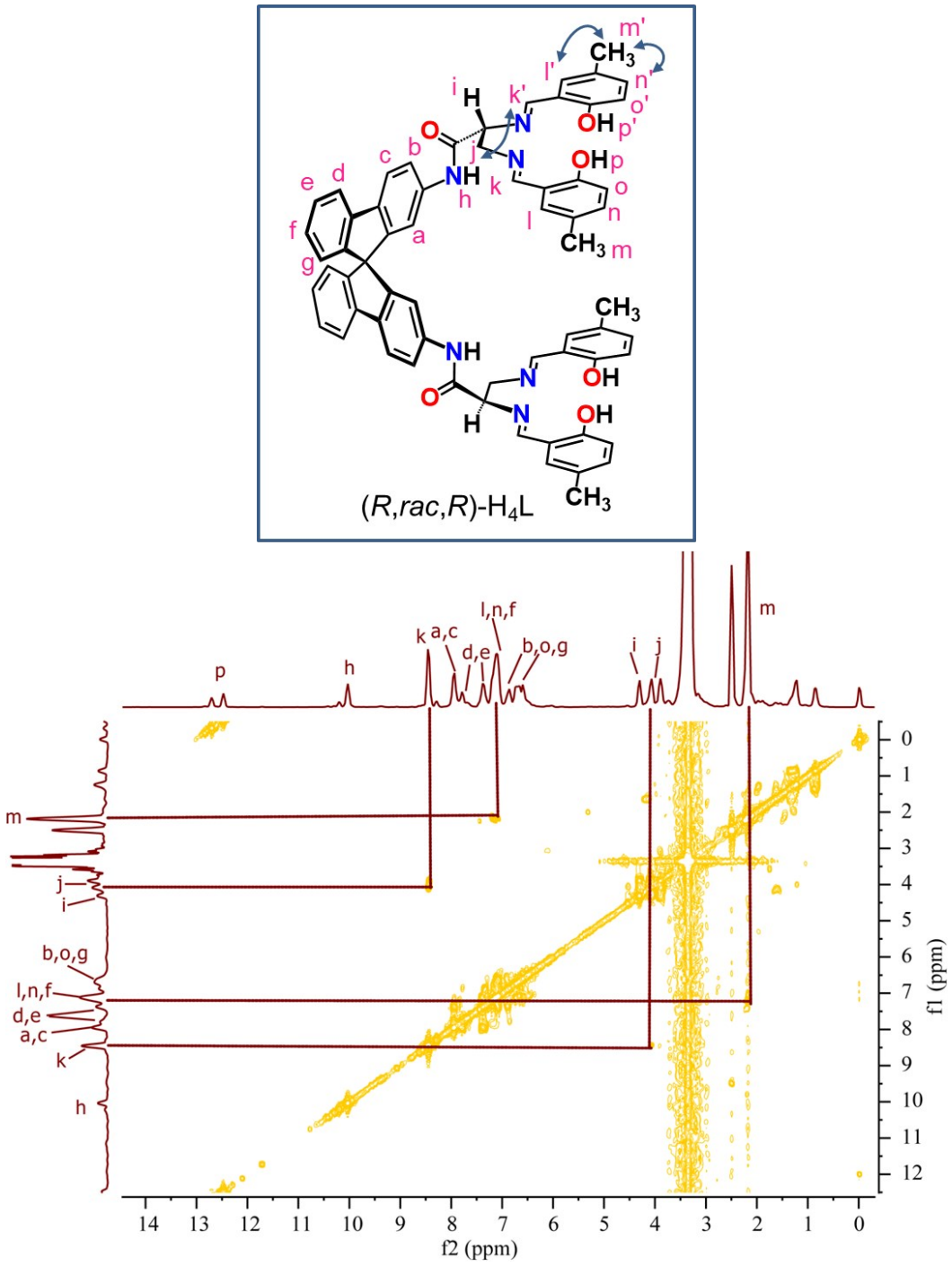

Figure S5. ^{1}H-^{1}H COSY spectrum of (*R,rac,R*)-H_4L (600 MHz, 5 mM, DMSO-d_6, 298 K). Inset shows the signal assignments.

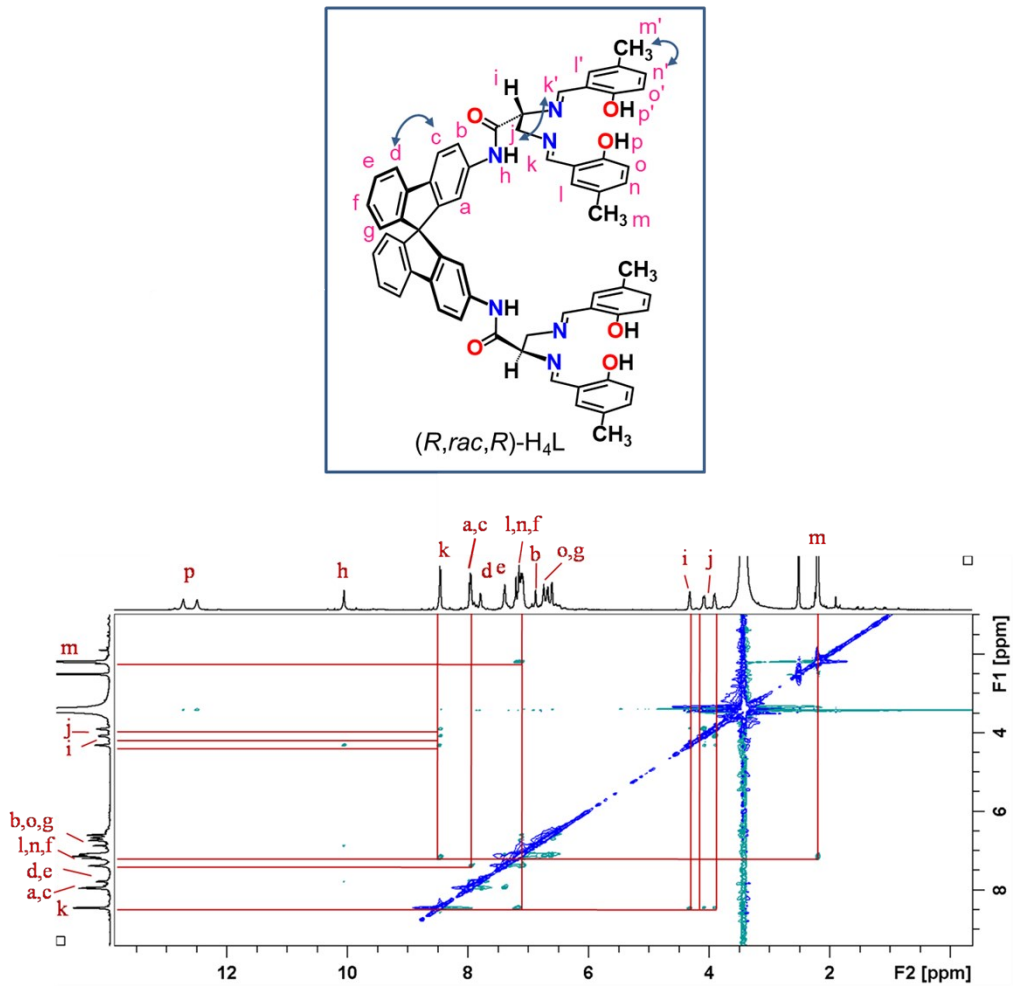

Figure S6. ^{1}H-^{1}H ROESY spectrum of (*R,rac,R*)-H_4L (600 MHz, 5 mM, DMSO-d_6, 298 K). Inset shows the signal assignments.

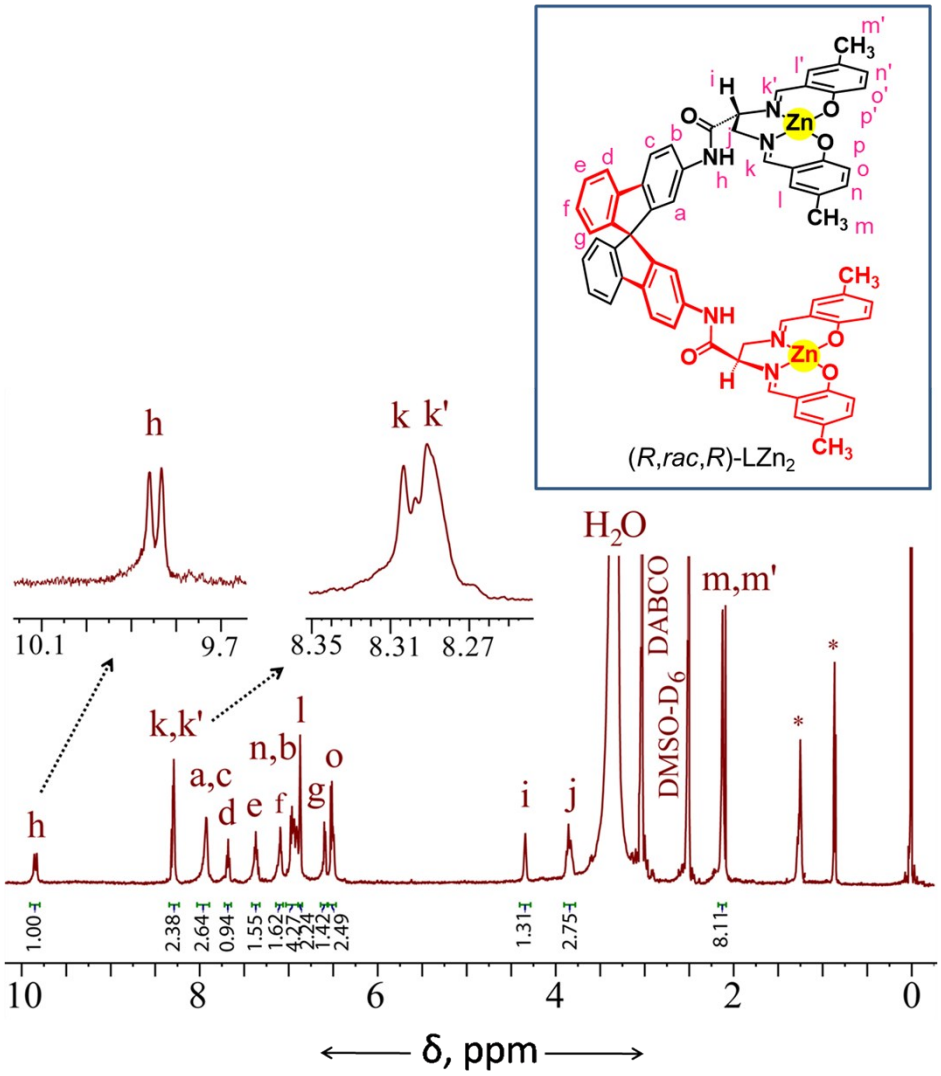

Figure S7. ^{1}H NMR spectrum of (*R,rac,R*)-LZn_2 (600 MHz, DMSO-d_6, 298 K). Inset shows the signal assignments. Asterisks denote solvent impurity.

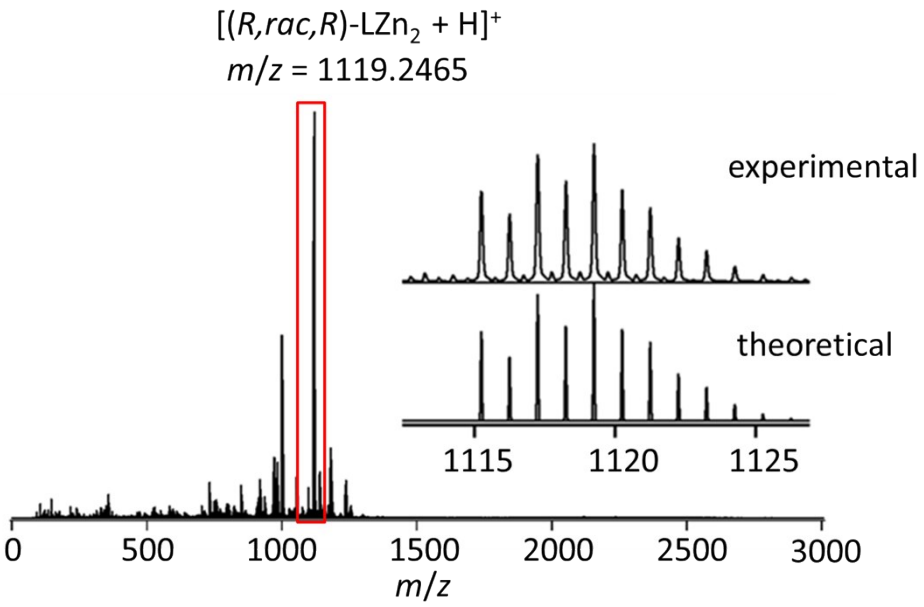

Figure S8. ESI-TOF mass spectrum of [(*R,rac,R*)-LZn_2] in CH_3CN in postitive mode. Inset shows the experimental and theoretical isotope patterns.

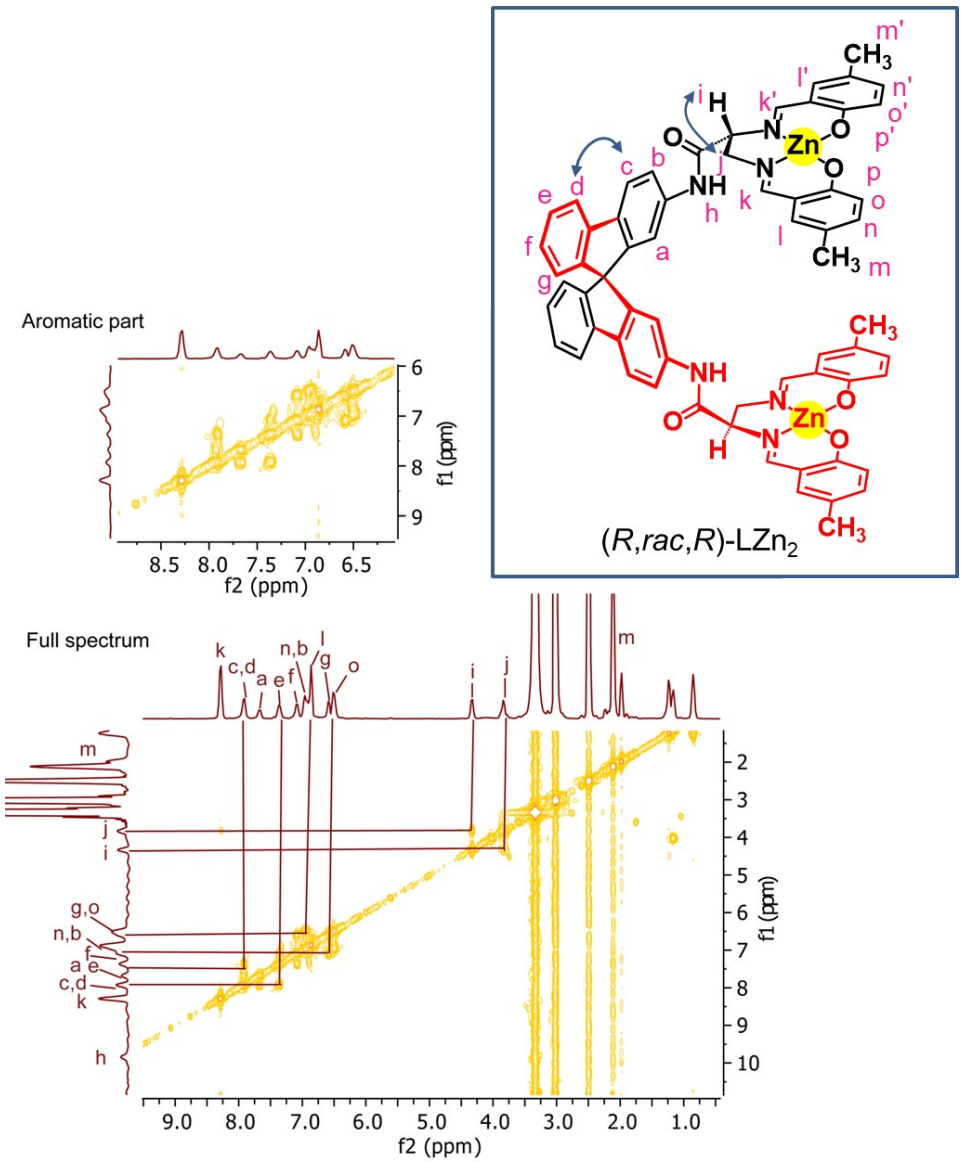

Figure S9. ^{1}H-^{1}H COSY spectrum of (*R,rac,R*)-LZn_2 (600 MHz, 5 mM, DMSO-d_6, 298 K). Inset shows the signal assignments.

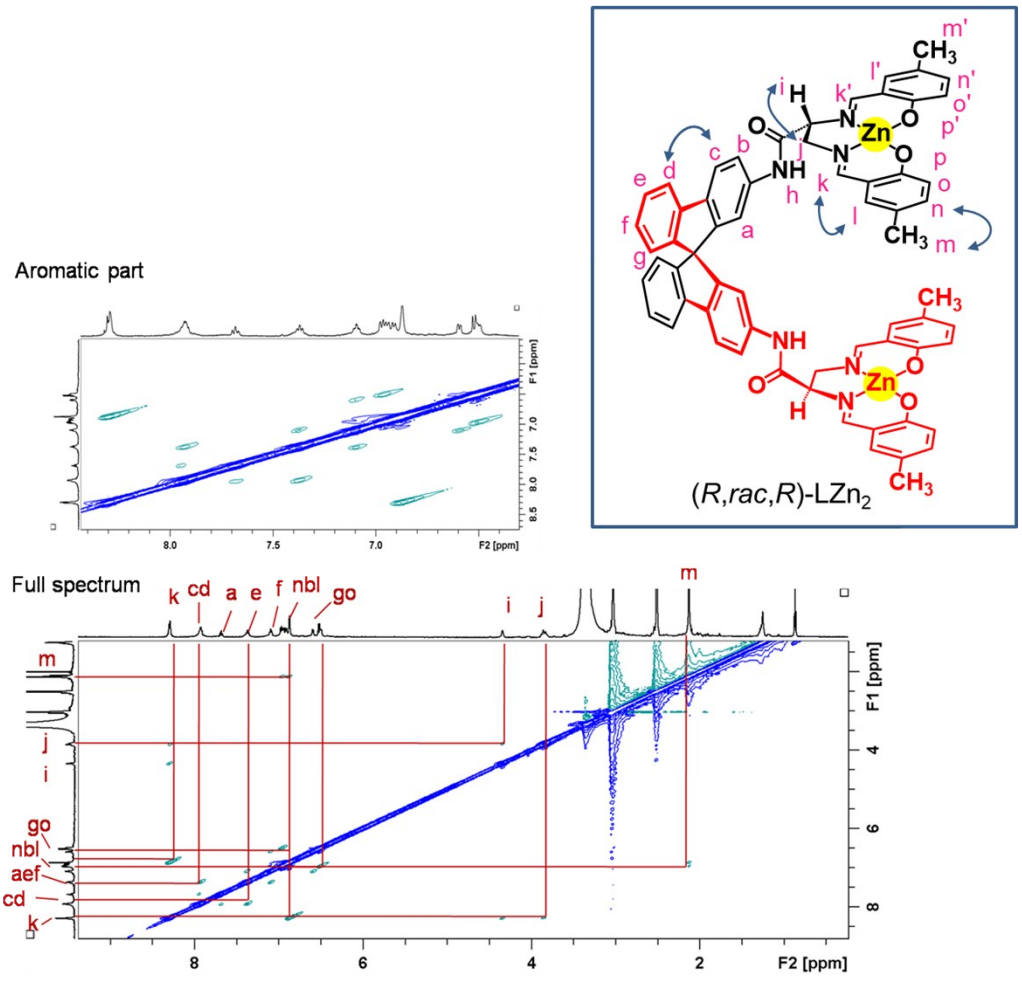

Figure S10. ^{1}H-^{1}H ROESY spectrum of (*R,rac,R*)-LZn$_2$ (600 MHz, 5 mM, DMSO-d_6, 298 K). Inset shows the signal assignments.

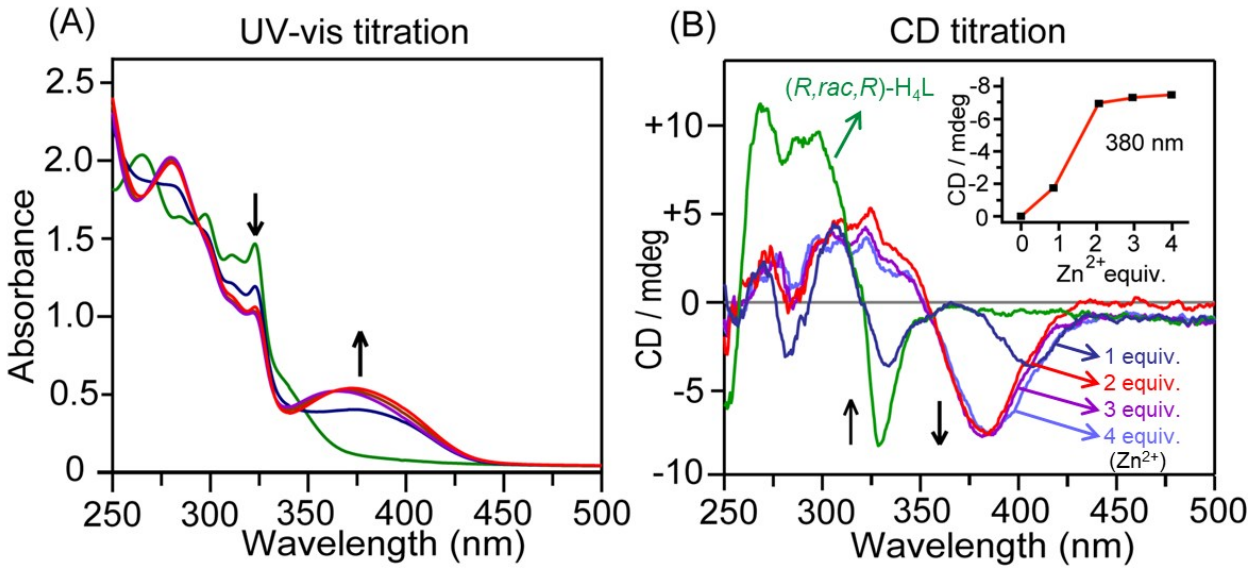

Figure S11. (A) UV-vis spectroscopic titration and (B) CD-spectroscopic titration of (*R,rac,R*)-H_4L (4.0×10^{-5} M) upon the addition of zinc(II) trifluoromethanesulfonate (up to 4.0 equiv) in $CHCl_3/CH_3CN$ (1:1) at 298 K.

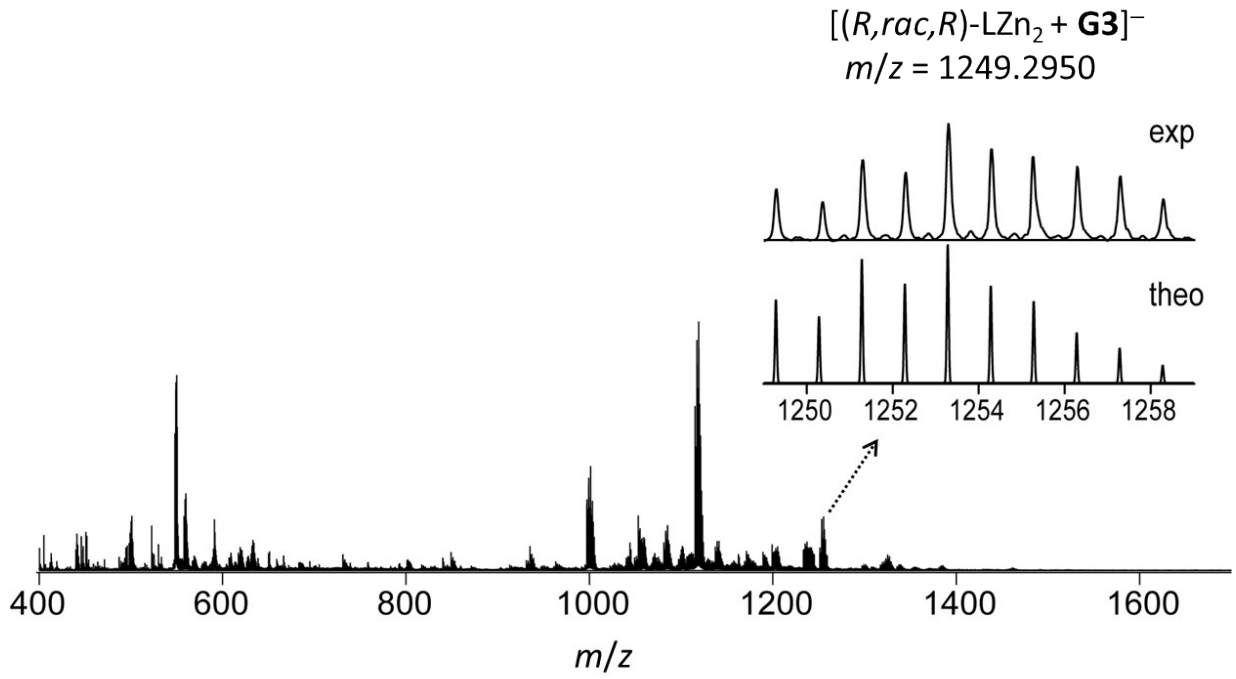

Figure S12. ESI-TOF mass spectrum of (*R,rac,R*)-Zn_2L upon addition of 1 equiv of **G3** in $CH_3CN/CHCl_3$ in negative mode. Inset shows the experimental and theoretical isotope patterns.

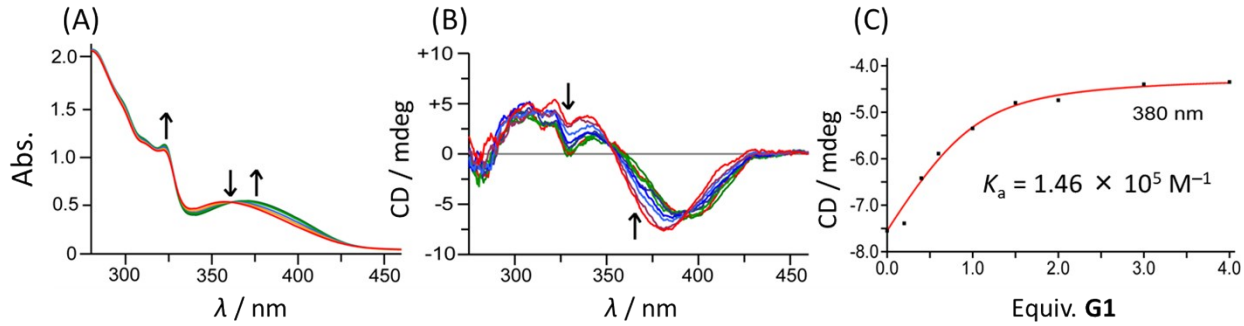

Figure S13. (A) UV-vis and (B) CD spectroscopic titrations of complex (*R*,*rac*,*R*)-LZn$_2$ (4.0 × 10^{-5} M) upon the addition of **G1** (4.0 equiv) in $CHCl_3$/CH_3CN (1:1) at 298 K; (C) CD spectroscopic titration curve and data fit at 380 nm.

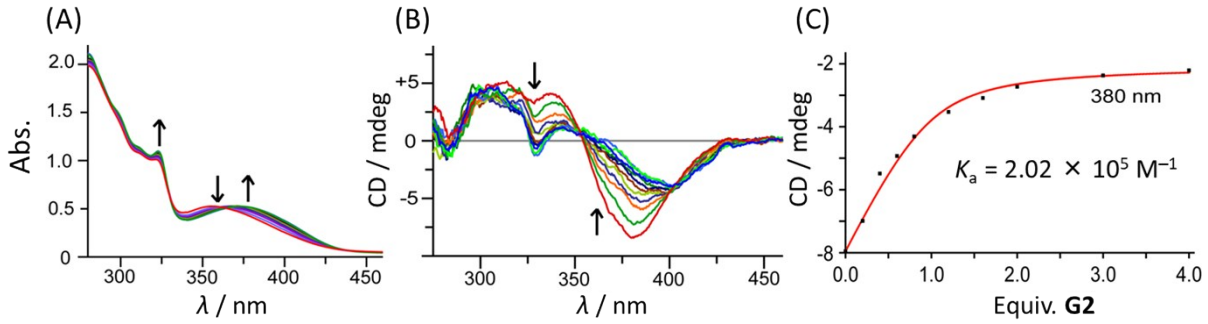

Figure S14. (A) UV-vis and (B) CD spectroscopic titrations of complex (*R*,*rac*,*R*)-LZn$_2$ (4.0 × 10^{-5} M) upon the addition of **G2** (4.0 equiv) in $CHCl_3$/CH_3CN (1:1) at 298 K; (C) CD spectroscopic titration curve and data fit at 380 nm.

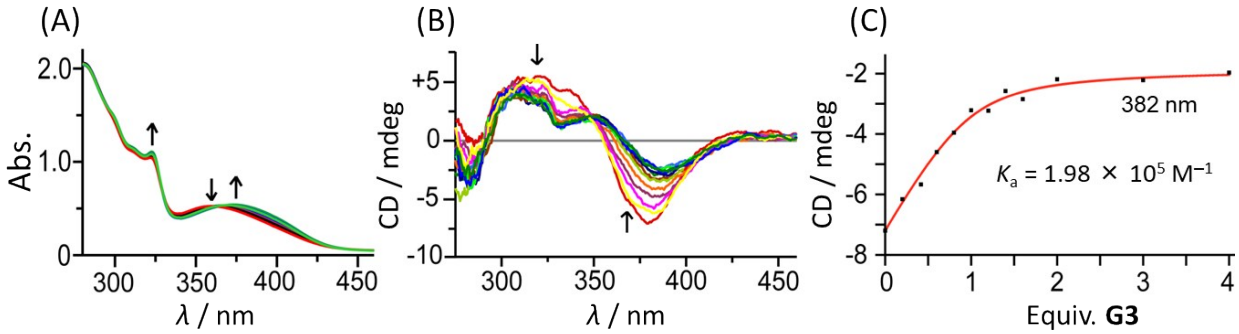

Figure S15. (A) UV-vis and (B) CD spectroscopic titrations of complex (*R*,*rac*,*R*)-LZn_2 (4.0 × 10^{-5} M) upon the addition of **G3** (4.0 equiv) in $CHCl_3/CH_3CN$ (1:1) at 298 K; (C) CD spectroscopic titration curve and data fit at 382 nm.

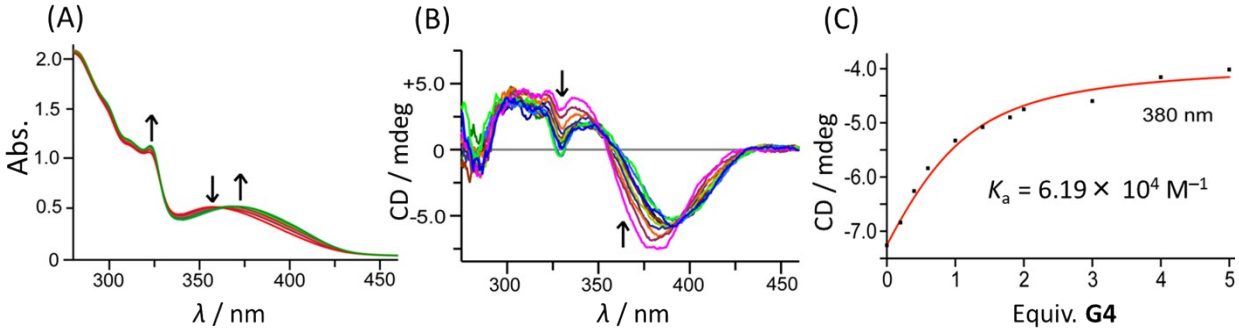

Figure S16. (A) UV-vis and (B) CD spectroscopic titrations of complex (*R*,*rac*,*R*)-LZn_2 (4.0 × 10^{-5} M) upon the addition of **G4** (5.0 equiv) in $CHCl_3/CH_3CN$ (1:1) at 298 K; (C) CD spectroscopic titration curve and data fit at 380 nm.

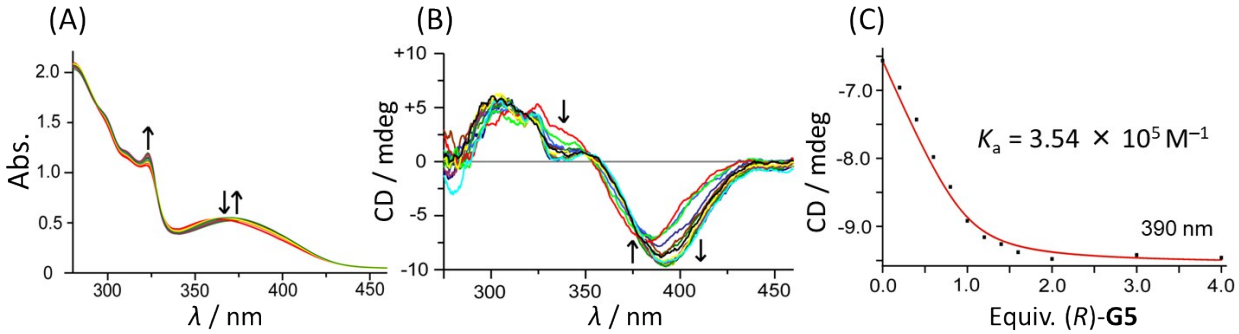

Figure S17. (A) UV-vis and (B) CD spectroscopic titrations of complex (*R*,*rac*,*R*)-LZn$_2$ (4.0 × 10^{-5} M) upon the addition of (*R*)-**G5** (4.0 equiv) in $CHCl_3$/CH_3CN (1:1) at 298 K; (C) CD spectroscopic titration curve and data fit at 390 nm.

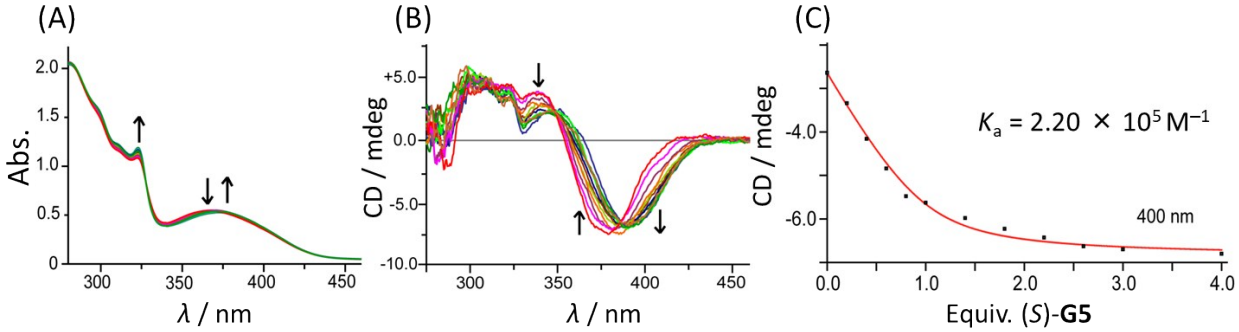

Figure S18. (A) UV-vis and (B) CD spectroscopic titrations of complex (*R*,*rac*,*R*)-LZn$_2$ (4.0 × 10^{-5} M) upon the addition of (*S*)-**G5** (4.0 equiv) in $CHCl_3$/CH_3CN (1:1) at 298 K; (C) CD spectroscopic titration curve and data fit at 400 nm.

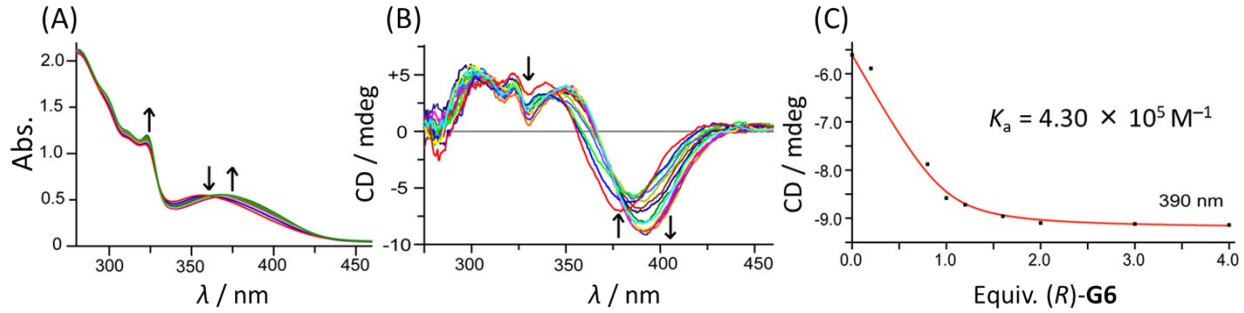

Figure S19. (A) UV-vis and (B) CD spectroscopic titrations of complex (*R*,*rac*,*R*)-LZn$_2$ (4.0 × 10^{-5} M) upon the addition of (*R*)-**G6** (4.0 equiv) in $CHCl_3$/CH_3CN (1:1) at 298 K; (C) CD spectroscopic titration curve and data fit at 390 nm.

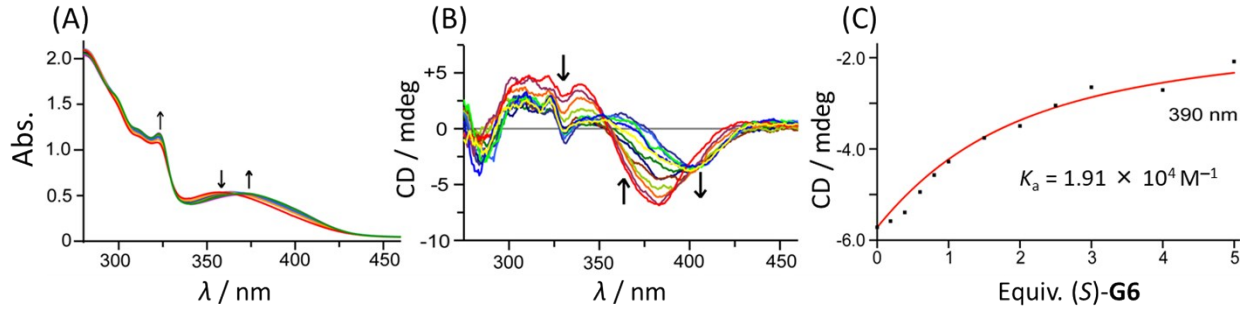

Figure S20. (A) UV-vis and (B) CD spectroscopic titrations of complex (*R*,*rac*,*R*)-LZn$_2$ (4.0 × 10^{-5} M) upon the addition of (*S*)-**G6** (5.0 equiv) in $CHCl_3$/CH_3CN (1:1) at 298 K; (C) CD spectroscopic titration curve and data fit at 390 nm.

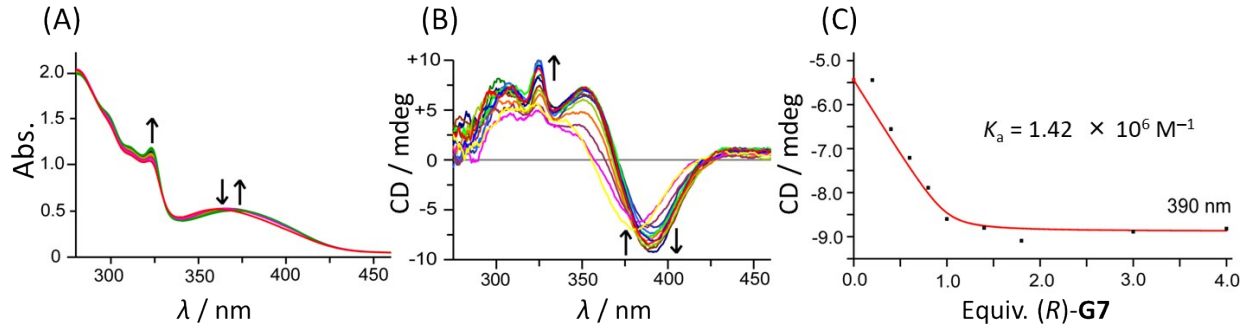

Figure S21. (A) UV-vis and (B) CD spectroscopic titrations of complex (*R*,*rac*,*R*)-LZn_2 (4.0×10^{-5} M) upon the addition of (*R*)-**G7** (4.0 equiv) in $CHCl_3/CH_3CN$ (1:1) at 298 K; (C) CD spectroscopic titration curve and data fit at 390 nm.

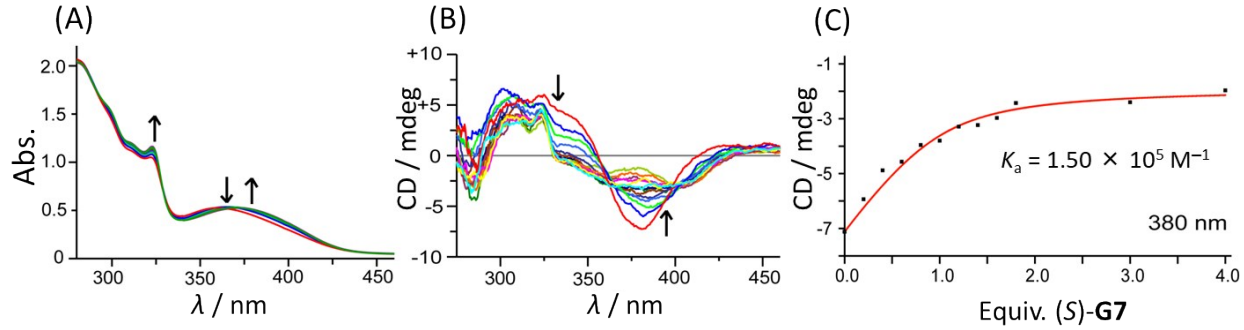

Figure S22. (A) UV-vis and (B) CD spectroscopic titrations of complex (*R*,*rac*,*R*)-LZn_2 (4.0×10^{-5} M) upon the addition of (*S*)-**G7** (5.0 equiv) in $CHCl_3/CH_3CN$ (1:1) at 298 K; (C) CD spectroscopic titration curve and data fit at 380 nm.

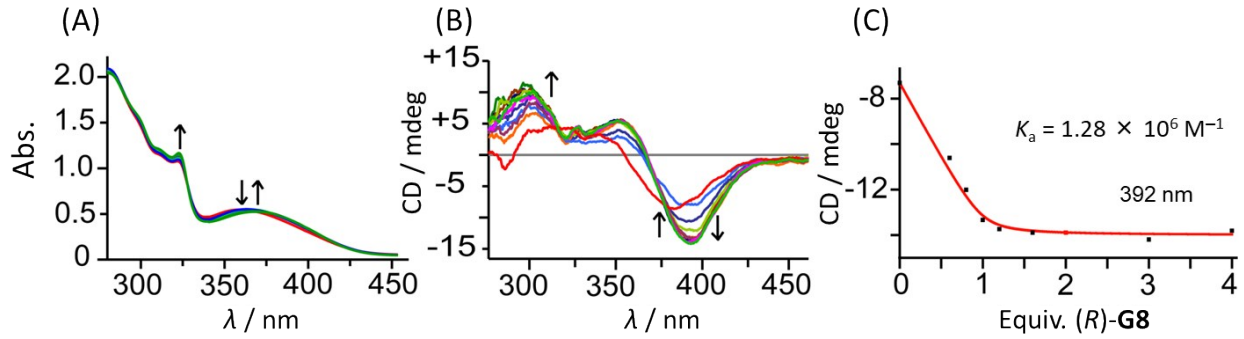

Figure S23. (A) UV-vis and (B) CD spectroscopic titrations of complex (*R*,*rac*,*R*)-LZn_2 (4.0 × 10^{-5} M) upon the addition of (*R*)-**G8** (4.0 equiv) in $CHCl_3/CH_3CN$ (1:1) at 298 K; (C) CD spectroscopic titration curve and data fit at 392 nm.

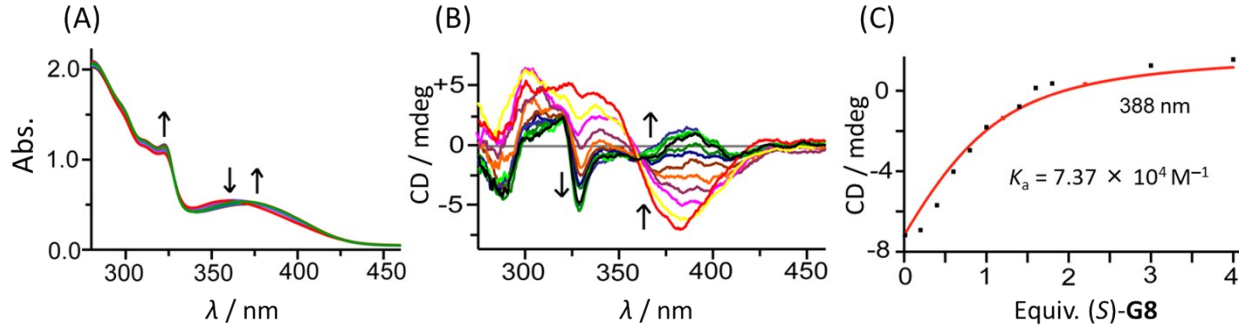

Figure S24. (A) UV-vis and (B) CD spectroscopic titrations of complex (*R*,*rac*,*R*)-LZn_2 (4.0 × 10^{-5} M) upon the addition of (*S*)-**G8** (4.0 equiv) in $CHCl_3/CH_3CN$ (1:1) at 298 K; (C) CD spectroscopic titration curve and data fit at 388 nm.

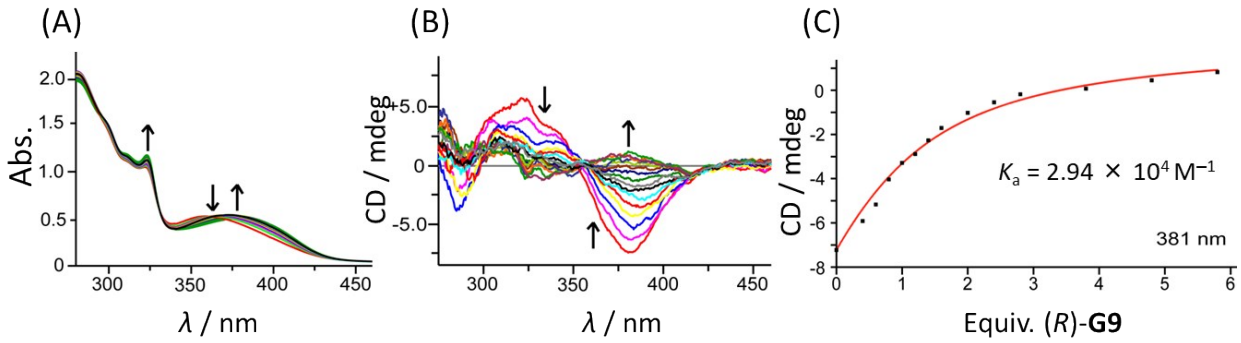

Figure S25. (A) UV-vis and (B) CD spectroscopic titrations of complex (*R*,*rac*,*R*)-LZn_2 (4.0 × 10^{-5} M) upon the addition of (*R*)-**G9** (6.0 equiv) in $CHCl_3/CH_3CN$ (1:1) at 298 K; (C) CD spectroscopic titration curve and data fit at 381 nm.

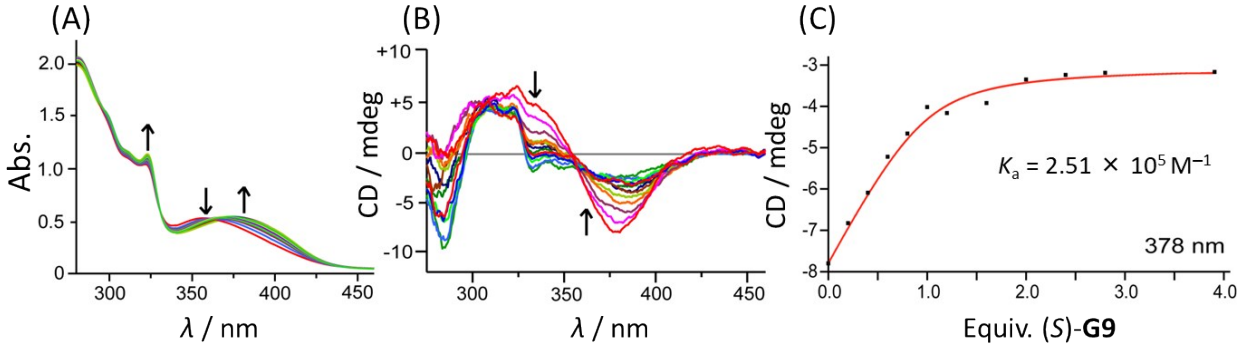

Figure S26. (A) UV-vis and (B) CD spectroscopic titrations of complex (*R*,*rac*,*R*)-LZn_2 (4.0 × 10^{-5} M) upon the addition of (*S*)-**G9** (4.0 equiv) in $CHCl_3/CH_3CN$ (1:1) at 298 K; (C) CD spectroscopic titration curve and data fit at 378 nm.

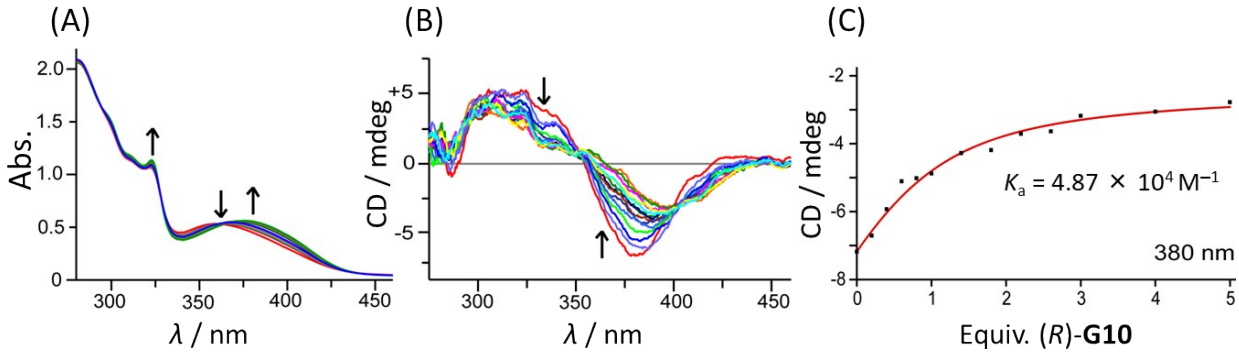

Figure S27. (A) UV-vis and (B) CD spectroscopic titrations of complex (*R*,*rac*,*R*)-LZn_2 (4.0×10^{-5} M) upon the addition of (*R*)-**G10** (5.0 equiv) in $CHCl_3/CH_3CN$ (1:1) at 298 K; (C) CD spectroscopic titration curve and data fit at 380 nm.

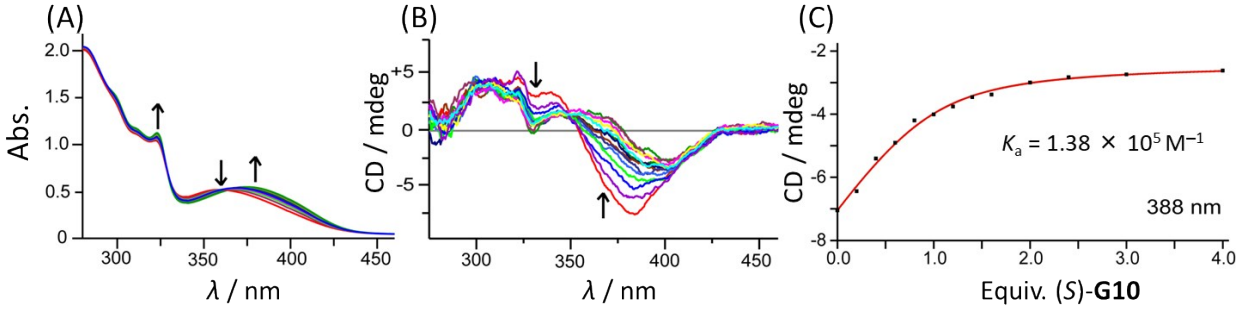

Figure S28. (A) UV-vis and (B) CD spectroscopic titrations of complex (*R*,*rac*,*R*)-LZn_2 (4.0×10^{-5} M) upon the addition of (*S*)-**G10** (4.0 equiv) in $CHCl_3/CH_3CN$ (1:1) at 298 K; (C) CD spectroscopic titration curve and data fit at 388 nm.

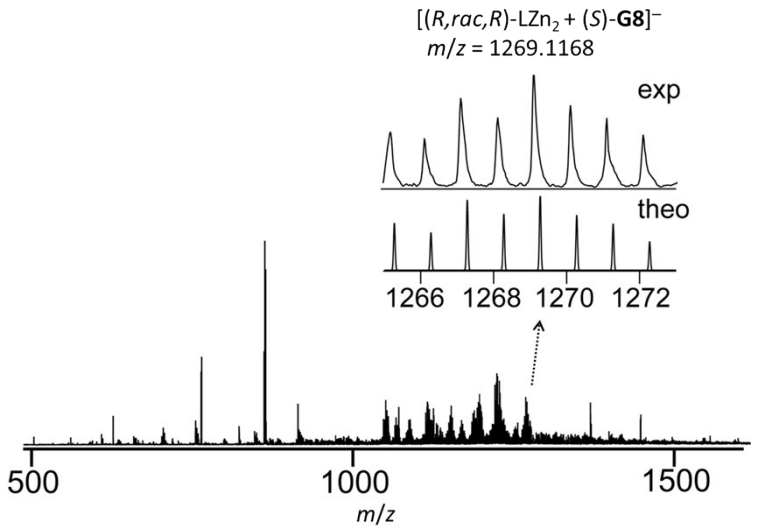

Figure S29. ESI-TOF mass spectrum of (*R,rac,R*)-LZn_2 in the presence of 1 equiv of (*S*)-**G8** in $CH_3CN/CHCl_3$ in negative mode. Inset shows the experimental and theoretical isotope patterns.

Table S1. CD spectral Data and Binding Constants of the Complexes in $CHCl_3/CH_3CN$ (1:1) at 298 K. [a]

Carboxylate guest	FC [b]		Binding constant K_a (M^{-1}) [c]	Enantioselectivity α [d]
	λ/nm	θ_{obs}/mdeg		
G1	396	–6.38	1.46×10^5	
G2	402	–3.90	2.02×10^5	
G3	388	–2.33	1.98×10^5	
G4	395	–5.10	6.19×10^4	
(*R*)-**G5**	392	–9.70	3.54×10^5	1.6 (*R*)
(*S*)-**G5**	392	–6.95	2.20×10^5	
(*R*)-**G6**	392	–9.11	4.30×10^5	22 (*R*)
(*S*)-**G6**	402	–3.37	1.91×10^4	
(*R*)-**G7**	391	–9.19	1.42×10^6	9.5 (*R*)
(*S*)-**G7**	381	–1.28	1.50×10^5	
(*R*)-**G8**	392	–14.21	1.28×10^6	17 (*R*)
(*S*)-**G8**	388	+1.36	7.37×10^4	
(*R*)-**G9**	381	+1.94	2.94×10^4	8.5 (*S*)
(*S*)-**G9**	378	–2.38	2.51×10^5	
(*R*)-**G10**	398	–2.63	4.87×10^4	2.8 (*S*)
(*S*)-**G10**	402	–2.78	1.38×10^5	

[a] CD spectral data measured after the addition of 4 equiv of carboxylate guests and 4 equiv of DABCO to the solution of (*R*,*rac*,*R*)-LZn_2 (4.0×10^{-5} M) in $CHCl_3/CH_3CN$ (1:1) at 298 K, path length = 10 mm.

[b] FC: first Cotton effect. The FC of (*R*,*rac*,*R*)-LZn_2 is –7.42 mdeg at 384 nm.

[c] Binding constants (K_a) determined from CD spectroscopic titration experiments.

[d] Enantioselectivity $\alpha = K_{a(R)}/K_{a(S)}$ and $K_{a(S)}/K_{a(R)}$ for (*R*) and (*S*) selectivity, respectively.